Polymer(Korea), Vol. 40, No. 2, pp. 238-244 (2016)
http://dx.doi.org/10.7317/pk.2016.40.2.238

ISSN 0379-153X(Print)
ISSN 2234-8077(Online)

투과도와 선택도 동시 향상 가능한 CO_2/N_2 분리용 P25/PVC-*g*-POEM 혼합매질 분리막

김상진 · 전하림 · 김동준 · 김종학†
연세대학교 화공생명공학과
(2015년 9월 26일 접수, 2015년 11월 2일 수정, 2015년 11월 7일 채택)

P25/PVC-*g*-POEM Mixed Matrix Membranes with Simultaneously Improved Permeability and Selectivity for CO_2/N_2 Separation

Sang Jin Kim, Harim Jeon, Dong Jun Kim, and Jong Hak Kim†
Department of Chemical and Biomolecular Engineering, Yonsei University, 50 Yonsei-ro, Seodaemun-gu, Seoul 03722, Korea
(Received September 26, 2015; Revised November 2, 2015; Accepted November 7, 2015)

초록: 일반적인 기체분리막은 투과도와 선택도의 역상관 관계를 가지고 있다. 본 연구에서는 P25(TiO_2 나노입자의 상품명)와 양친성 가지형 공중합체로 구성된 혼합매질을 제조하였으며 투과도와 선택도가 동시 향상되는 결과를 얻었다. 가지형 공중합체는 폴리비닐클로라이드(PVC) 주사슬과 폴리옥시에틸렌메타크릴레이트(POEM) 곁사슬로 구성되었으며 원자전달라디칼중합(ATRP)을 통해 합성하였다. DSC 결과를 통해 P25를 도입했을 경우 PVC-*g*-POEM의 유리전이온도가 감소되는 것을 확인하였으며 이는 사슬 결정도의 감소를 나타낸다. XRD, SAXS, TGA, SEM을 통해 분리막의 결정 구조, 도메인간의 간격 변화, 미세 모폴로지 및 열적 특성을 분석하였다. 순수 PVC-*g*-POEM에 비해, P25/PVC-*g*-POEM 혼합매질 분리막은 투과도는 46.2에서 102.8 Barrer(1 Barrer=1×10^{-10} cm^3(STP)·cm·cm^{-2}·s^{-1}·$cmHg^{-1}$)로 122% 증가하였으며, CO_2/N_2 선택도는 29.6에서 39.1로 32% 향상되었다. 증가된 CO_2 투과도는 증가된 확산도의 결과이며, 향상된 선택도는 N_2 용해도 감소로부터 기인한다.

Abstract: Conventional gas separation membranes have a trade-off relation between permeability and selectivity. Here, we report simultaneously improved permeability and selectivity through a mixed matrix membrane (MMM) consisting of P25 and amphiphilic graft copolymer. A graft copolymer composed of poly(vinyl chloride) (PVC) and poly(oxyethylene methacrylate) (POEM) as the backbone and side chains, respectively, was synthesized. The glass transition temperature (T_g) of PVC-*g*-POEM decreased upon addition of P25, indicating a decrease in chain rigidity. The crystalline structure, d-spacing, morphology and thermal properties of membranes were characterized by X-ray diffraction (XRD), small angle X-ray scattering (SAXS), thermogravimetric analysis (TGA), and scanning electron microscopy (SEM). Compared to pristine PVC-*g*-POEM, the CO_2 permeability through P25/PVC-*g*-POEM MMM increased by 122% from 46.2 to 102.8 Barrer, while the CO_2/N_2 selectivity increased by 32% from 29.6 to 39.1. The increased CO_2 permeability mostly resulted from increased diffusivity, while the increased selectivity was attributed to decreased solubility of N_2.

Keywords: CO_2, gas separation, mixed matrix membrane, TiO_2, graft copolymer.

Introduction

Gas separation membranes are promising materials that can potentially be used to diminish greenhouse gas emissions from fossil fuel combustion, which is contributing to global climate change. Among emitted gases, carbon dioxide (CO_2) is considered the main culprit of the greenhouse effect, and thus separation of CO_2 from flue gas is critical. Separation of CO_2 from N_2 is usually carried out in the post-combustion process.[1-3] Typical separation technology involves use of an amine solution but is expensive and consumes a large amount of energy[4,5] compared to membrane processes, which are simple to perform and cost-effective.[6-10] Polymeric membranes have been widely investigated and used for gas separation; however, the upper bound trade-off relationship between gas permeability and selectivity remains a barrier. There has been intense investigation of polymers with different structures and morphologies in an attempt to approach the upper bound trade-off

†To whom correspondence should be addressed.
E-mail: jonghak@yonsei.ac.kr

relation in polymeric membranes.[11]

Introduction of inorganic filler into the polymer matrix, which results in a mixed matrix membrane (MMM), represents a breakthrough in gas separation research.[12-20] TiO_2 nanoparticles (P25) have been incorporated into glassy polymers such as polyimide or poly(1-trimethylsilyl-1-propyne) to form MMMs.[21-23] However, the interfacial contact between glassy polymers and rigid inorganic nanoparticles is poor, resulting in the formation of interfacial voids that allow for easy passage of gas molecules, leading to loss of selectivity. Rubbery polymers are considered good alternatives for MMMs, but their use has been limited by their poor mechanical strength. Thus, development of polymers with good mechanical strength and good interfacial contact with the inorganic filler is important.

Poly(ethylene oxide) (PEO) has received much attention as a polymer membrane to separate CO_2 due to the strong affinity of ether oxygens in PEO for CO_2.[24-26] This specific interaction leads to high selective solubility of CO_2 in PEO, resulting in high permselectivity. However, the helical structure of PEO chains results in high crystallinity, which reduces gas permeability. Poly(oxyethylene methacrylate) (POEM) is amorphous PEO without crystallinity, but its poor mechanical strength, manifested by its sticky, fluidic properties, has limited its use in gas separation membranes. To address these issues, microphase-separated nanostructural block copolymers such as PEBAX, which is the trade name of poly(amide-*b*-ethylene oxide) block copolymer, have been employed.[27-32] However, block copolymers are typically synthesized via living anionic polymerization, which is highly sensitive to impurities such as H_2O and O_2, making it expensive to perform.

In this study, we fabricated a MMM with P25 as a filler and a low-cost amphiphilic graft copolymer as a matrix. Atom transfer radical polymerization (ATRP) was utilized to synthesize graft copolymer consisting of a poly(vinyl chloride) (PVC) backbone and poly(oxyethylene methacrylate) (POEM) side chains.[33-35] P25-containing PVC-*g*-POEM MMMs were characterized by X-ray diffraction (XRD), small angle X-ray scattering (SAXS), differential scanning calorimetry (DSC), thermogravimetric analysis (TGA), and scanning electron microscopy (SEM). Pure gas permeation properties were measured using the time lag method at 35 °C.

Experimental

Materials. Poly(vinyl chloride) (PVC, M_n=99000 g/mol), poly(oxyethylene methacrylate) (POEM, poly(ethylene glycol) methyl ether methacrylate, M_n=475 g/mol), 1,1,4,7,10,10-hexamethyltriethylene tetramine (HMTETA, 99%), and copper(I) chloride (CuCl, 99%) were purchased from Aldrich. Tetrahydrofuran (THF), *N*-methyl pyrrolidone (NMP), and methanol were obtained from J.T. Baker. P25 (TiO_2 nanopowder, 21 nm) was also purchased from Aldrich. All chemicals were reagent grade and used as-received.

Synthesis of PVC-*g*-POEM Graft Copolymer. ATRP procedure was utilized to synthesize PVC-*g*-POEM graft copolymer.[31-33] 3 g of PVC were added to 50 mL of NMP and stirred vigorously at room temperature for 1 day for complete dissolution of the polymer. After a homogeneous polymer solution was obtained, 0.05 g of CuCl, 9 mL of POEM, and 0.12 mL of HMTETA were added in sequence. After the solution turned green, it was purged with nitrogen to get rid of the residual oxygen in the flask, which is necessary for ATRP polymerization. The polymerization reaction was carried out at 90 °C for 24 h. After polymerization, the resultant mixtures were precipitated into methanol more than three times and dried in a 50 °C oven overnight. Then, the mixtures were dried again in a vacuum oven overnight at room temperature.

Preparation of Membranes. PVC-*g*-POEM graft copolymer was dissolved in THF to prepare polymer solution, while P25 powder was dispersed in THF by ultrasonication and magnetic stirring separately. The ratio of P25 to PVC-*g*-POEM was fixed at 1:1 wt. The homogeneously dissolved polymer solution was mixed with the P25 solution and mixed by magnetic stirring for 1 day. After sufficient stirring, the mixed solution was poured in glass petri-dish and dried at room temperature overnight. For complete removal of residual solvent, the casted mixture film was dried again in a vacuum oven at 50 °C for 1 day. Film thickness was approximately 60 μm.

Characterization. The crystalline structure of membranes was characterized using X-ray diffraction (XRD, D8 Advance, Bruker, Germany) with Cu Kα radiation (λ=1.5406 Å). The D8 system was operated at 40 kV and 40 mA. The 2θ range was varied from 5° to 70° with a scanning speed of 2°/min. The morphologies of membranes were observed using a field-emission scanning electron microscope (FE-SEM, JEOL 6701F, JEOL Ltd). To investigate the thermal properties of membranes, differential scanning calorimetry (DSC, DSC-Q1000, TA Instruments, UK) was used and samples were heated from -80 to 250 °C at a rate of 10 °C/min. Degradation of membranes was measured as a function of temperature via thermogravimetric analysis (TGA, Q-5000 IR, TA Instruments,

USA) with a heating rate of 10 °C/min from 50 to 700 °C. SAXS data were obtained with the 4C SAXS II beamline at the Pohang Accelerator Laboratory (PAL), Korea.

Gas Permeability Measurements. Pure gas permeation properties were determined using a constant volume/variable pressure apparatus provided by Airrane Co. Ltd. (Korea) according to our previously reported method.[36,37] The leak rate in the system was measured before starting the permeation experiments and afterward, the pressure increase in the downstream volume was recorded to determine permeability. Gas permeability was calculated from the steady-state rate of the pressure increase in a fixed downstream volume. Downstream pressure was always less than 2 torr, which was much lower than the upstream pressure. The average estimated error of gas permeability was approximately ±2%. The diffusivity (D) or diffusion coefficient was determined from the time-lag (θ), which is the period of time to reach the steady state and the intercept in x-axis of the plot (pressure vs. time), using the following equation: $D=L^2/6\theta$, where L is membrane thickness. Solubility (S) or the solubility coefficient can then be calculated from the permeability, P, and D by the equation $P=D\times S$.

Results and Discussion

An important consideration when fabricating high performance MMMs is correct pairing of the inorganic filler and organic polymer matrix to ensure good interfacial properties. In this study, we synthesized an amphiphilic PVC-*g*-POEM graft copolymer via ATRP and used an organic polymer matrix. Direct initiation of the secondary chlorines of PVC was preceded by formation of a graft copolymer consisting of PVC main chains and POEM side chains using Cu/ligand complex as a catalyst. It should be noted that graft copolymer is preferable to block copolymer as a nanostructural copolymer because of the low cost and ease of synthesis of the former. The glassy, hydrophobic properties of the PVC main chain improve the mechanical strength of the membranes, while the rubbery, hydrophilic POEM side chains increase CO_2 solubility and therefore CO_2 permeability. Figure 1 shows the appearance of (a) neat PVC-*g*-POEM graft copolymer film and (b) P25/PVC-*g*-POEM MMM. Neat PVC-*g*-POEM membrane was brownish in color and highly transparent, while P25-containing MMM was translucent compared to the neat polymer membrane. This was due to light scattering at the interface of P25 and PVC-*g*-POEM because of their different refractive indices.

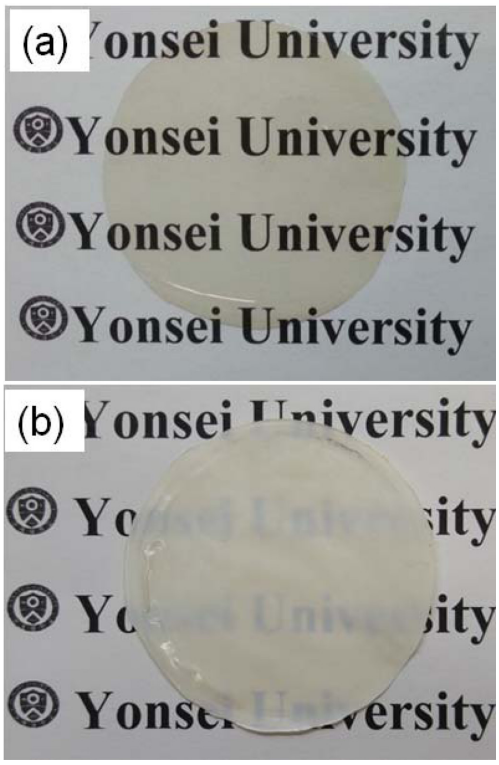

Figure 1. Photographs of (a) neat PVC-*g*-POEM membrane; (b) P25/PVC-*g*-POEM MMM.

Figure 2 shows the surface and cross-sectional morphology of P25/PVC-*g*-POEM MMM observed via FE-SEM. The SEM image of the membrane surface revealed that the P25 nanoparticles, which had a diameter of approximately 20 nm, were homogenously dispersed throughout the polymer matrix without severe aggregation of particles. The magnified surface image shows that the interfacial adhesion between the PVC-*g*-POEM matrix and the P25 filler was strong and dense. Although small pores (size of a few angstroms), which are responsible for gas molecule sieving, cannot be confirmed by SEM analysis, the absence of severe interfacial voids or cracks, which can cause a significant decrease in gas selectivity, was confirmed. Good interfacial properties and homogenous dispersion of filler were further confirmed by a cross-sectional SEM image of the MMM.

The crystal structure of P25-containing PVC-*g*-POEM MMM was determined by XRD measurements and compared with that of pristine PVC-*g*-POEM graft copolymer, as shown in Figure 3, in which X-ray intensity is plotted as a function of 2θ. The XRD pattern of neat PVC-*g*-POEM graft copolymer exhibits a broad main peak centered at 19.0° and a shoulder at

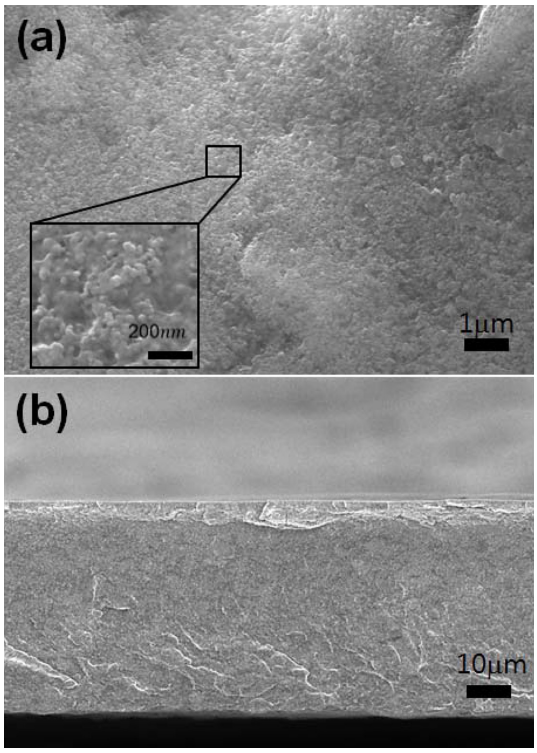

Figure 2. (a) Surface; (b) cross-sectional SEM images of P25/PVC-*g*-POEM MMM.

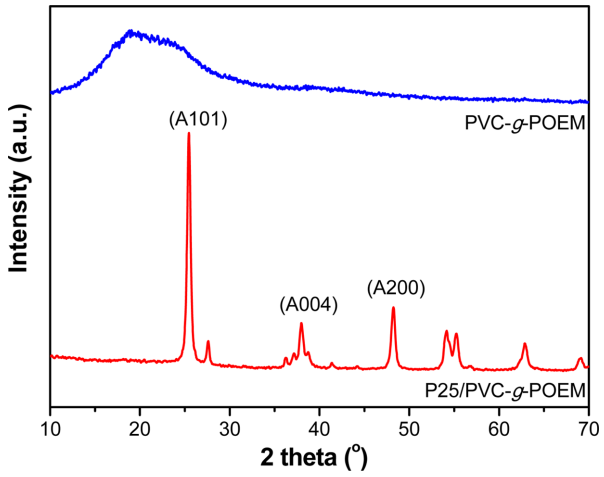

Figure 3. XRD patterns of neat PVC-*g*-POEM membrane and P25/PVC-*g*-POEM MMM.

23.2°. The absence of sharp peak indicates that the PVC-*g*-POEM graft copolymer is fully amorphous. The existence of two maximum peaks indicates that the PVC-*g*-POEM graft copolymer has bimodal d-spacing. Using the Bragg relation, the d-spacing value was calculated to be 4.6 and 3.8 Å based on 2θ=19.0° and 23.2°, respectively. For MMM containing

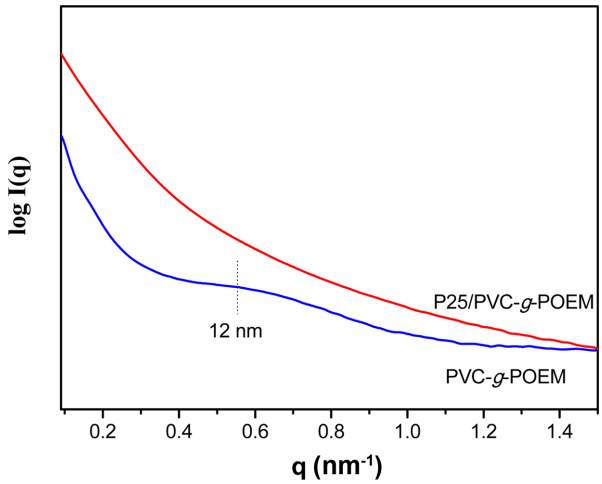

Figure 4. SAXS curves of neat PVC-*g*-POEM membrane and P25/PVC-*g*-POEM MMM.

P25, the broad amorphous peak of PVC-*g*-POEM almost completely disappeared and only crystalline peaks of P25 nanoparticles are observed. Strong peaks observed at 25.3°, 38.0°, 48.2° corresponded to the (101), (004), and (200) planes of anatase TiO_2, respectively (ICDD-JCPDS no. 86-1157). The average crystallite size of TiO_2 was determined to be 19 nm, which might enable better dispersion in the polymer matrix. The XRD results indicate that due to homogenous dispersion of highly crystalline P25, the polymer matrix had decreased amorphous properties, and the MMM was crystalline.

Figure 4 shows SAXS plots of neat PVC-*g*-POEM and P25/PVC-*g*-POEM MMM, in which intensity is plotted as a function of the q value (nm^{-1}). The neat PVC-*g*-POEM membrane curve has a small shoulder peak at q=0.53 nm^{-1}, corresponding to d-spacing of 12.0 nm ($d=2\pi/q$), which indicates the average distance between PVC chains of the graft copolymer. The broad peak of the neat PVC-*g*-POEM polymer weakened and is hardly observed in P25/PVC-*g*-POEM MMM, indicating the breakup of the initial microphase-separated structure of the polymer matrix.

DSC measurements of membranes were taken to analyze thermal property changes, especially the glass transition temperature (T_g) shift, as shown in Figure 5. The DSC curve of neat PVC-*g*-POEM copolymer exhibits two distinct T_g values at 40 °C and -60 °C due to the motions of the PVC and POEM segments, respectively. The existence of two distinctive T_gs without an endothermic melting temperature indicates that the PVC-*g*-POEM graft copolymer is fully amorphous and microphase-separated, consistent with the XRD results. The DSC curve of P25/PVC-*g*-POEM MMM shows T_g value slightly

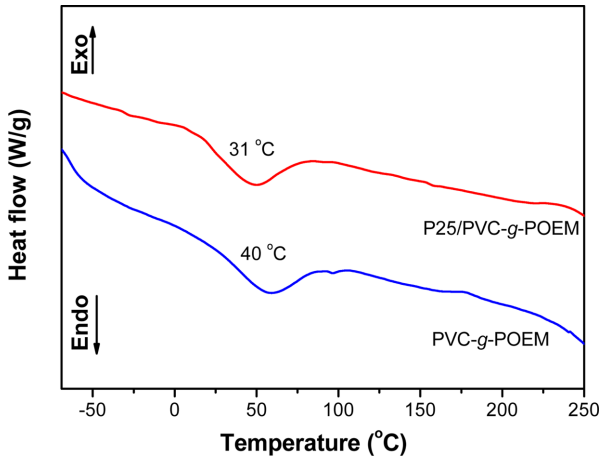

Figure 5. DSC curves of neat PVC-*g*-POEM membrane and P25/PVC-*g*-POEM MMM.

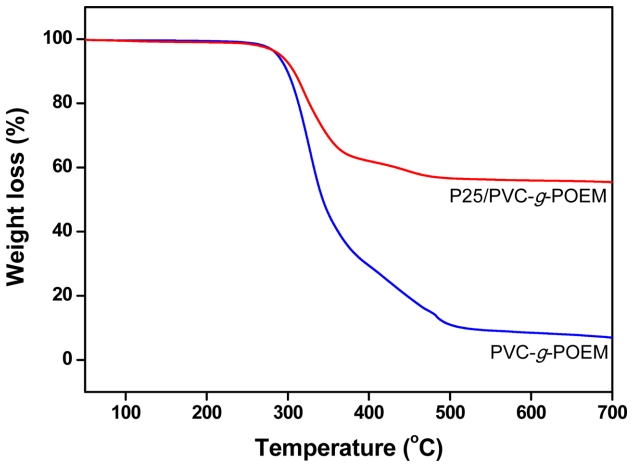

Figure 6. TGA results of neat PVC-*g*-POEM membrane and P25/PVC-*g*-POEM MMM.

shifted toward the lower temperature of 31 °C from 40 °C, which indicates a decrease in chain rigidity of the polymer matrix. This thermal property change likely occurred due to the presence of homogeneously dispersed and trapped P25 nanoparticles between the polymer chains, which might have reduced the bonding strength of inter/intra chains and thus

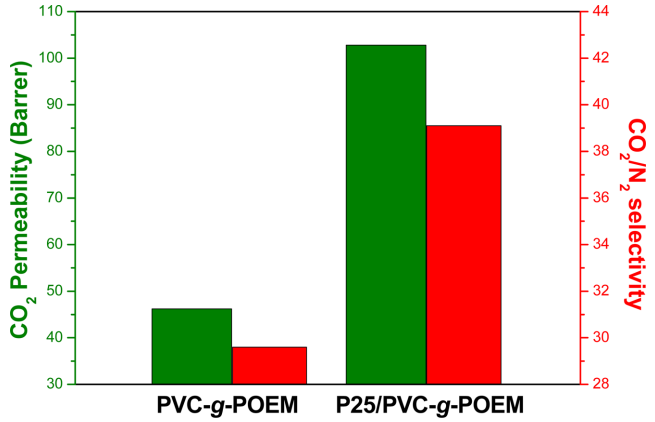

Figure 7. CO_2 permeability and CO_2/N_2 selectivity through neat PVC-*g*-POEM membrane and P25/PVC-*g*-POEM MMM.

acted as a plasticizer to decrease T_g.

To investigate the thermal stability of the membranes, TGA analysis was performed as shown in Figure 6. There is no weight loss up to 300 °C; however, above, this temperature, a two-step degradation pattern is observed for both membrane types. The weight loss that occurred over the temperature range of 300~350 °C accounted for about 70% of the total weight loss, and we attributed this to degradation of the flexible POEM segment in the PVC-*g*-POEM graft copolymer.[33] The second degradation step over the temperature range of 350~500 °C accounts for about 30% of the total weight loss; we attributed this to degradation of the rigid PVC backbone. Together, these findings indicate that introduction of P25 did not affect the thermal stability of the membranes. The composition of P25 in the MMM was confirmed to be 50 wt%; this end-point value was identical to the feed amount.

The gas permeation properties of the membranes with respect to CO_2 and N_2 in addition to CO_2/N_2 ideal selectivity were assessed via the time-lag method using a constant volume/variable pressure apparatus at 35 °C (Figure 7, Table 1). As can be seen from the gas permeation results, amphiphilic PVC-*g*-POEM graft copolymer is an excellent matrix material. The CO_2 permeability of the PVC-*g*-POEM graft copolymer

Table 1. Pure Gas Permeability and CO_2/N_2 Selectivity through Neat PVC-*g*-POEM Membrane and P25/PVC-*g*-POEM MMM at 35 °C

	Permeability (Barrer, 10^{-10} cm^3(STP)·cm/cm^2·s·cmHg)		Diffusivity (10^{-7} cm^2/s)		Solubility (10^{-1} cm^3(STP)/cm^3·cmHg)		Selectivity		
	N_2	CO_2	N_2	CO_2	N_2	CO_2	P_{CO2}/P_{N2}	D_{CO2}/D_{N2}	S_{CO2}/S_{N2}
PVC-*g*-POEM	1.6	46.2	3.02	1.36	0.0053	0.340	29.6	0.45	64.2
P25/PVC-*g*-POEM	2.6	102.8	5.78	3.03	0.0045	0.339	39.1	0.52	75.3

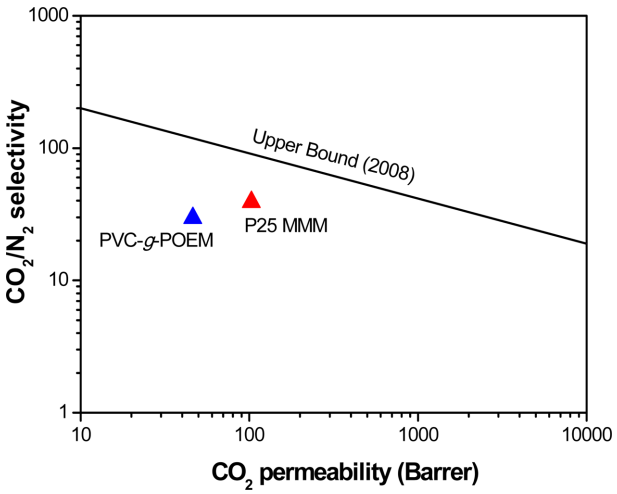

Figure 8. CO_2 permeability vs. CO_2/N_2 selectivity with an upper bound line (2008).

was 46.2 Barrer (1 Barrer=1×10^{-10} cm^3 (STP)· $cm\cdot cm^{-2}\cdot s^{-1}\cdot cmHg^{-1}$), while the CO_2/ N_2 permselectivity of the membrane was 29.6. The mechanical strength of the membrane was provided by the high molecular weight of the glassy PVC polymer backbone. Furthermore, grafting of POEM, which has good CO_2 affinity through dipole-quadrupole interactions, enhanced the CO_2 permeability of the membrane.[36-39] The introduction of P25 into the PVC-*g*-POEM graft copolymer resulted in a simultaneous increase in CO_2 permeability and CO_2/N_2 selectivity compared to the neat PVC-*g*-POEM membrane. The CO_2 permeability of P25/PVC-*g*-POEM MMM increased by 122% from 46.2 to 102.8 Barrer, while the CO_2/ N_2 selectivity increased from 29.6 to 39.1. The improved CO_2 permeability might have been due to increased gas diffusivity from the free volume increase that resulted from introduction of P25 into the polymer matrix. Homogeneously dispersed P25 in the polymer matrix might have functioned like a plasticizer to disrupt the alignment of polymer chains and thus increase chain mobility. This is consistent with the DSC analysis, which shows a shift in the T_g value to a lower temperature, implying a decrease in chain rigidity. To determine the exact factors responsible for an improvement in gas separation performance, the gas diffusivity and solubility of the MMMs were also analyzed. Table 1 shows the gas separation properties of the MMMs. CO_2 diffusivity of P25/PVC-*g*-POEM MMM almost doubled from 1.36×10^{-7} to 3.03×10^{-7} cm^2/s; however the CO_2 solubility of MMM shows only a slight drop from 0.0340 to 0.0339 $cm^3(STP)/cm^3\cdot cmHg$. The diffusivity of N_2 also increased with the addition of P25 to PVC-*g*-POEM. Due to the slightly greater improvement in CO_2 diffusivity than N_2 diffusivity, the diffusivity selectivity of MMM barely increased. Analysis of gas diffusivity properties and DSC results indicate that introduction of P25 nanoparticles, which were homogeneously dispersed in the overall polymer matrix, resulted in trapping of the P25 nanoparticles in the polymer chains and disruption of chain-chain interaction. These factors in turn increased the chain mobility of the polymer matrix and facilitated the transport of gas molecules. Figure 8 shows the gas separation properties of P25-based MMMs as well as the upper bound line (2008), which shows the trade-off relation between permeability and selectivity. Introduction of P25 into the PVC-*g*-POEM polymer increased the CO_2 permeability to 102.8 Barrer with a simultaneous increase in selectivity compared to bare PVC-*g*-POEM membrane. This result indicates that the upper bound line (1991) was surpassed and located slightly under the upper bound (2008). Composite membranes are of interest as they are more cost effective than free-standing dense membranes. If the P25/PVC-*g*-POEM MMM is deposited as the top layer on an appropriate porous bottom support with 1 μm thickness, the high CO_2 permeance of 102.8 GPU could be obtained, which will be investigated in the near future.

Conclusions

We investigated the structural and gas separation properties of MMMs containing P25 based on an amphiphilic PVC-*g*-POEM graft copolymer. The amphiphilic PVC-*g*-POEM graft copolymer was synthesized via ATRP process and used as the matrix of the MMM. Thermal property analysis via DSC measurements revealed that the T_g of the P25/PVC-*g*-POEM MMM was lower than that of neat PVC-*g*-POEM polymer, which implied an increase in chain mobility in the MMM. Higher chain mobility and increased free volume fraction of polymer matrix results in better CO_2 diffusivity, which we confirmed through gas separation property measurements. The CO_2 permeability of P25/PVC-*g*-POEM MMM compared to neat PVC-*g*-POEM polymer increased by 122% from 46.2 to 102.8 Barrer, and CO_2/N_2 selectivity also increased by 32% from 29.6 to 39.1. Gas permeation analysis revealed that the CO_2 diffusivity of P25/PVC-*g*-POEM MMM increased from 1.36×10^{-7} (neat PVC-*g*-POEM polymer) to 3.03×10^{-7} cm^2/s, while CO_2 solubility remained unchanged. This result indicated that an increase in CO_2 diffusivity via an improvement in chain mobility and free volume fraction of polymer matrix was the main factor responsible for the increased gas permeability

of P25/PVC-*g*-POEM MMM relative to neat PVC-*g*-POEM polymer.

Acknowledgements: This work was supported by the Human Resources Program in Energy Technology (20154010200810), and the Energy Efficiency & Resources (20122010100040) of the Korea Institute of Energy Technology Evaluation and Planning (KETEP).

References

1. M. Saeed and L. Deng, *J. Membr. Sci.*, **494**, 196 (2015).
2. J. Zhao, Z. Wang, J. Wang, and S. Wang, *J. Membr. Sci.*, **403**, 203 (2012).
3. T. C. Merkel, H. Lin, X. Wei, and R. Baker, *J. Membr. Sci.*, **359**, 126 (2010).
4. J. D. Figueroa, T. Fout, S. Plasynski, H. McIlvried, and R. D. Srivastava, *Int. J. Greenh. Gas Control*, **2**, 9 (2008).
5. E. S. Rubin, C. Chen, and A. B. Rao, *Energy Policy*, **35**, 4444 (2007).
6. Y.-M. Kwon, H.-G. Im, and J.-H. Kim, *Polym. Korea*, **34**, 1 (2010).
7. K. L. Gleason, Z. P. Smith, Q. Liu, D. R. Paul, and B. D. Freeman, *J. Membr. Sci.*, **475**, 204 (2015).
8. M. Zhou, D. Korelskiy, P. Ye, M. Grahn, and J. Hedlund, *Angew. Chem. Int. Ed.*, **53**, 3492 (2014).
9. E. H. Cho, K. B. Kim, and J. W. Rhim, *Polym. Korea*, **38**, 687 (2014).
10. D.-H. Kim, H.-S. Im, M.-S. Kim, B.-S. Lee, B.-S. Lee, S.-W. Yoon, B.-S. Kim, Y.-I. Park, S.-I. Cheong, and J.-W. Rhim, *Polym. Korea*, **33**, 537 (2009).
11. L. M. Robeson, *J. Membr. Sci.*, **320**, 390 (2008).
12. M. A. Semsarzadeh, B. Ghalei, M. Fardi, M. Esmaeeli, and E. Vakili, *Korean J. Chem. Eng.*, **31**, 841 (2014).
13. T. Yang and T. S. Chung, *Int. J. Hydrogen Energy*, **38**, 229 (2013).
14. H. Y. Zhao, Z. Jin, H. M. Su, J. L. Zhang, X. D. Yao, H. J. Zhao, and G. S. Zhu, *Chem. Commun*., **49**, 2780 (2013).
15. T.-S. Chung, L.Y. Jiang, Y. Li, and S. Kulprathipanja, *Prog. Polym. Sci*., **32**, 483 (2007).
16. P. Burmann, B. Zornoza, C. Téllez, and J. Coronas, *Chem. Eng. Sci*., **107**, 66 (2014).
17. M. Arjmandi, M. Pakizeh and O. Pirouzram, *Korean J. Chem. Eng.*, **32**, 1178 (2015).
18. S. Kanehashi, G. Q. Chen, C. A. Scholes, B. Ozcelik, C. Hua, L. Ciddor, P. D. Southon, D. M. D'Alessandro, and S. E. Kentish, *J. Membr. Sci.*, **482**, 49 (2015).
19. T. B. Kang and S. R. Hong, *Membr. J.*, **25**, 295 (2015).
20. S. G. Kim and T. B. Kang, *Membr. J.*, **25**, 27 (2015).
21. Y. Kong, H. Du, J. Yang, D. Shi, Y. Wang, Y. Zhang, and W. Xin, *Desalination*, **146**, 49 (2002).
22. S. Matteucci, V. A. Kusuma, D. Sanders, S. Swinnea, and B. D. Freeman, *J. Membr. Sci.*, **307**, 196 (2008).
23. F. Moghadam, M. R. Omidkhah, E. Vasheghani-Farahani, M. Z. Pedram, and F. Dorosti, *Sep. Purif. Technol.*, **77**, 128 (2011).
24. A. Tena, A. Marcos-Fernández, A. E. Lozano, J. de Abajo, L. Palacio, P. Prádanos, and A. Hernández, *Chem. Eng. Sci.*, **104**, 574 (2013).
25. A. Tena, A. Marcos-Fernández, L. Palacio, P. Prádanos, A. E. Lozano, J. de Abajo, and A. Hernández, *J. Membr. Sci.*, **434**, 26 (2013).
26. L. Kwisnek, J. Goetz, K. P. Meyers, S. R. Heinz, J. S. Wiggins, and S. Nazarenko, *Macromolecules*, **47**, 3243 (2014).
27. M. M. Rahman, V. Filiz, S. Shishatskiy, C. Abetz, S. Neumann, S. Bolmer, M. M. Khan, and V. Abetz, *J. Membr. Sci.*, **437**, 286 (2013).
28. V. Nafisi and M.-B. Hägg, *J. Membr. Sci.*, **459**, 244 (2014).
29. V. Nafisi and M.-B. Hägg, *ACS Appl. Mater. Interfaces*, **6**, 15643 (2014).
30. H. Rabiee, M. Soltanieh, S. A. Mousavi, and A. Ghadimi, *J. Membr. Sci.*, **469**, 43 (2014).
31. S. Wang, Y. Liu, S. Huang, H. Wu, Y. Li, Z. Tian, and Z. Jiang, *J. Membr. Sci.*, **460**, 62 (2014).
32. P. Bernardo, J. C. Jansen, F. Bazzarelli, F. Tasselli, A. Fuoco, K. Friess, P. Izák, V. Jarmarová, M. Kačírková, and G. Clarizia, *Sep. Purif. Technol.*, **97**, 73 (2012).
33. D. K. Roh, S. J. Kim, W. S. Chi, J. K. Kim, and J. H. Kim, *Chem. Commun.*, **50**, 5717 (2014).
34. S. H. Ahn, D. J. Kim, W. S. Chi, and J. H. Kim, *Adv. Funct. Mater.*, **24,** 5037 (2014).
35. S. H. Ahn, D. J. Kim, W. S. Chi, and J. H. Kim, *Adv. Mater.,* **25**, 4893 (2013).
36. W. S. Chi, S. J. Kim, S. J. Lee, Y. S. Bae, and J. H. Kim, *Chem. Sus. Chem*., **8**, 650 (2015).
37. W. S. Chi, S. Hwang, S.-J. Lee, S. Park, Y.-S. Bae, D.Y. Ryu, J. H. Kim, and J. Kim, *J. Membr. Sci.*, **495**, 479 (2015).
38. H. Rabiee, A. Ghadimi, and T. Mohammadi, *J. Membr. Sci.*, **476**, 286 (2015).
39. K. Bierbrauer, M. López-González, E. Riande, and C. Mijangos, *J. Membr. Sci.*, **362**, 164 (2010).